Desalination and Water Treatment
www.deswater.com
doi: 10.5004/dwt.2020.26022

198 (2020) 41–52
September

Analysis of a novel humidification–dehumidification desalination system

Avhad Pankaj Baban, Shankar Krishnan*

Department of Mechanical Engineering, Indian Institute of Technology Bombay, Powai, Mumbai – 400 076, Maharashtra, India, emails: kshankar@iitb.ac.in (S. Krishnan), pankajavhad2391@gmail.com (A.P. Baban)

Received 17 October 2019; Accepted 24 April 2020

ABSTRACT

This paper reports on mathematical modeling and experimental demonstration of a compact humidification–dehumidification (HDH) system. The HDH system studied here consists of a humidifier where the air is humidified and a dehumidifier where externally heated moist air condenses. The latent heat of condensation is recovered via a common-conducting heat transfer wall shared between the humidifier and the dehumidifier. For the present study, a bubble-column dehumidifier is investigated, while falling film air-water counter-flow configuration is considered as a humidifier. Condensed produce water is collected at the dehumidifier, and brine is rejected at the water outlet of the humidifier. In this paper, a modified heat exchanger analysis is reported that accounts for a volumetrically uniform heat source due to condensation in the dehumidifier. The analysis also accounts for co-current air-water vapor flow from an evaporating stream of water. Heat and mass transfer in the wet evaporating channel is analogous to that in a cooling tower. The model is able to predict the variation of the temperature difference between the humidifier and the bubble column condenser as a function of the vertical distance of the shared wall. Gained-output-ratio (system energy efficiency) is quantified using the model developed and compared against simple prototype HDH experiments in an open-air open-water configuration. Finally, the utility of the mathematical analysis and deduced results are discussed.

Keywords: Humidification–dehumidification; Desalination; Dewvaporation; Heat exchanger

1. Introduction

Humidification–dehumidification (HDH) desalination technology appears to be a promising approach for decentralized, low-cost drinking water production if energy cost for water production is reduced. As per World Bank data, the population of India has increased three times within the last 55 y, but rainfall in India has not increased in proportion, and it is not sufficient for current needs. Several parts of India are under water-stressed, water-scarce, or absolute water scarcity category because in 1 y (8,760 h), maximum precipitation received is approximately 100 h. Growing population, inefficient use of the groundwater resources, water/capita/y decreased from 6,008 to 1,545 m^3 in 2011. Of the 575,000 Indian villages, about 162,000 face problems of brackish or contaminated water, and scarcity of freshwater [1]. Based on the UNICEF report [1], a population of 1,210 million was affected by water shortage in 2011 and a projected population of 1,394 million in 2025. Fifty-four percent of India faces high to extremely high water stress. Based on the principle of operation, desalination technologies may be classified as membrane-based, thermal-based, and alternate technologies. The first category consists of technologies that utilize membranes for separation of water from a saline feed, and the second includes those that utilize thermal energy for separation of water from a saline feed. Those technologies that separate salt using mechanisms different from the membrane and thermal gradients are classified as alternate technologies. Examples include capacitive deionization, ion-concentration polarization, and

* Corresponding author.

1944-3994/1944-3986 © 2020 Desalination Publications. All rights reserved.

others. Among the membrane technologies, reverse osmosis is widely adopted. Reverse osmosis (RO) desalination is a known but expensive solution for decentralized water production where regular maintenance and pre-processing of the feed water are needed [2]. Likewise, thermal desalination technologies such as multi-effect distillation, multi-stage flash, and their variants are commonly known to produce distilled water [2]; but, are an expensive approach for decentralized small-scale desalination plants. The key challenge in realizing these technologies is to make them low cost, to provide them at a community-scale or smaller (0.5–100 m^3 of water), and relatively maintenance-free.

HDH desalination, a non-traditional desalination technology, is a potential candidate for decentralized water production at a small-scale if its energy efficiency can be improved [3]. In a typical water heated open-air open-water HDH system, ambient air enters the humidifier, and preheated water flows in a counter-flow fashion. In the humidifier, due to simultaneous heat and mass transfer, hot water transfers water vapor to flowing air while exchanging heat. Following humidification of air in the humidifier, the moist hot air enters a dehumidifier where it condenses. Condensation is achieved utilizing the incoming cold saline feed stream using a heat exchanger. Saline water, on the other hand, cools and condenses the hot moist air and recovers thermal energy. Subsequently, the preheated stream is heated by a heater, and the heated water enters the humidifier.

The heating of the water stream can be achieved by using electrical energy, solar, geothermal, and others. Narayan et al. [4] reviewed solar-based HDH desalination systems and compared their performance. The basis of comparison was the HDH cycle heating configurations, which could either be water heated or air heated cycles. The most energy-efficient solar HDH system was found to be the multi-effect closed-air open-water cycle. The review concluded that there is a need for more research in order to improve the HDH system efficiency and realize its full economic potential to produce fresh water. A number of new innovative ideas for solar-driven HDH have been explored by researchers. To mention a few: direct absorption bubble column humidifier [5], parabolic trough [6], reflectors [7], and other novel ideas are discussed here [8,9]. Beyond solar-driven cycles, investigators have explored geothermal energy to power HDH systems. Ghalavand et al. [10] explored geothermal energy to heat saline feed water, and they investigated the effect of feed water-to-airflow ratio variation, the impact of cooling water temperature on distillate produced, and temperature of geothermal heat source at heat exchanger inlet. Recent advances in HDH desalination technology in terms of improved designs and system productivity focuses on improving individual component-level heat and mass transfer [11–13], the impact of carrier gases [14] as well as improving the heat recovery within the system [15–17]. Theoretical estimations of gained-output-ratio (GOR) for HDH is ~122 [18]. But, the demonstrated systems have shown to be about 4.5 at best. Hence, much scope for performance improvement exists for HDH systems. It is well-known that one of the key factors for improving the GOR of HDH systems is to design systems that enable improved heat integration/reuse.

Hamieh and Beckman [19–21] introduced the concept of dewvaporation desalination. In the dewvaporation technique, humidification and dehumidification processes were carried in one continuous contact tower with thermal energy from the condensation process is recovered for humidification of the incoming stream. External heat sources such as solar energy or fuel combustion can be used as heat input to the system. Hamieh et al. [20] have performed mathematical analysis, experimental demonstration as well as economic analysis and showed that high heat recovery could be achieved via the dewvaporation concept. Theoretical values obtained from their model illustrates a GOR as high as 9.5 for seawater feed and up to 16.8 for brackish water. These values indicate the possibility of this system to compete with large-scale thermal desalination technologies like multiple-effect distillation and multi-stage flash distillation on the basis of energy consumption. Ranganathan [22] recently proposed the development of a solar-powered dewvaporation system for seawater desalination. One of the critical issues of the dewvaporation technique is the requirement of a large area for condensation if the conventional condenser is used, that is, if condensation occurs on a cold surface. It is well-known that in the presence of noncondensable gas, the thermal resistance to water vapor condensation on a cold surface is much higher compared to a pure vapor condensation [23].

Lienhard et al. [3,18,24,25] proposed and demonstrated bubble-column condensers for dehumidification of humidifier air. Dehumidification is particularly challenging for HDH systems due to the presence of noncondensable gases along with water vapor. They demonstrated that very high fluxes, and hence heat transfer coefficients, can be dissipated in bubble column condensers. The impact is compactness that can be achieved, which is of particular interest in this work. The multi-stage bubble column enhances energy recovery by reducing the temperature drop between successive stages but adds complexity, cost, and maintenance [18]. While bubble column condensers are relatively new, but bubble column reactors are commonly used in the case of highly exothermic reactions in the liquid phase [26] and have been shown to 100 times higher heat transfer coefficients compared to single-phase systems.

In this work, we propose to combine the dewvaporation technique with the bubble-column condenser to enable a compact small-scale desalination system. Fig. 1 shows the schematic of our proposed HDH system concept. While the schematic shows a simple humidifier with a single-stage bubble column concept, the concept proposed here can be easily extended to multi-stage bubble columns with a packed bed humidifier. In the humidifier, the air is supplied from the bottom, and saline water is fed from the top, and as the air rises up, it is humidified due to heat and mass transfer from the counter-flowing water. This moist air is heated or mixed with saturated steam, if available, to increase the humid air temperature. This high-temperature humid air is bubbled through the bubble column where the moisture condenses in the distillate, which is periodically tapped out. The heat of condensation from the condenser is transferred to the humidifier to evaporate the incoming saline water stream that flows along the partitioning wall. The arrangement of humidifier and dehumidifier in

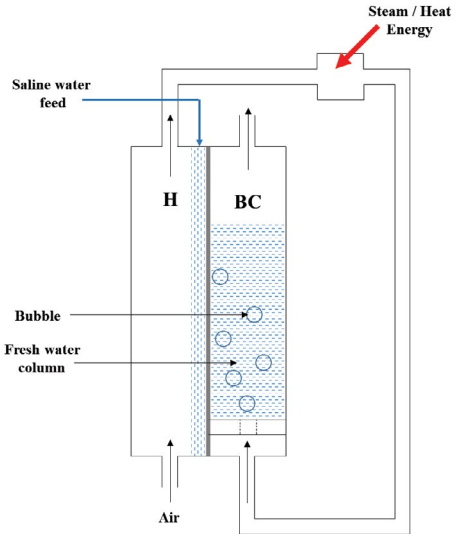

Fig. 1. Schematic of an HDH system considered in this work.

the proposed concept illustrates a co-flow of air and water streams in the system in an open-air open-water configuration. We first develop simplified mathematical modeling of the system concept, and then custom prototype set-up was built and performance measured. For mathematical modeling, we develop a framework that combines the modeling of indirect evaporative heat exchanger [27] along with modified heat exchanger analysis that accounts for heat source term in one of the streams [28].

2. Mathematical modeling

In the following sub-sections, first modeling of humidifier and bubble column dehumidifiers are considered separately, and then system-level modeling is developed.

2.1. Humidifier

In the humidifier of the HDH system, saline water is fed from the top and flows down along the partitioning wall as a liquid film. Air flows in the counter-flow direction. Thermal energy supplied across the wall from the condenser drives the heating and evaporation of water. Heat transfer from the falling water film to counter flowing air stream is driven by the enthalpy difference between the air stream and saturated water–air interface. It involves simultaneous sensible and latent heat transfer. During evaporation, both sensible and latent heat transfer takes place and can be expressed as:

$$dQ_H = \mathrm{d}Q_{\text{sensible}} + dQ_{\text{latent}} \tag{1}$$

$$dQ_{\text{sensible}} = \bar{h}_1 dA\left(T_2 - T_1\right) \tag{2}$$

where T_1 and T_2 are the temperatures of the air stream and water-film, as shown in Fig. 4a. Latent heat transfer can be expressed as:

$$dQ_{\text{latent}} = \bar{h}_m dA\left(\omega_2 - \omega_1\right) h_{\text{fg}} \tag{3}$$

Lewis factor [29] is the ratio of heat transfer Stanton number to mass transfer Stanton number and is given as:

$$\text{Le}_f = \frac{\text{St}}{\text{St}_m} = \frac{\dfrac{\bar{h}}{\rho u C_{p_{\text{ma}}}}}{\dfrac{\bar{h}_m}{\rho u}} = \frac{\bar{h}}{\bar{h}_m C_{p_{\text{ma}}}} \tag{4}$$

$$\bar{h}_m = \frac{\bar{h}_1}{\text{Le}_f C_{p_{\text{ma}}}} \tag{5}$$

As discussed in Kloppers and Kröger [29], assuming $\text{Le}_f \approx 1$ for air–water mixture, we obtain:

$$\bar{h}_m = \frac{\bar{h}_1}{C_{p_{\text{ma}}}} \tag{6}$$

Putting Eqs. (6) in (3), we get:

$$dQ_{\text{latent}} = \frac{\bar{h}_1}{C_{p_{\text{ma}}}} dA\left(\omega_2 - \omega_1\right) h_{\text{fg}} \tag{7}$$

On substituting Eqs. (2) and (7) in Eq. (1), we obtain:

$$dQ_H = \bar{h}_1 dA\left(T_2 - T_1\right) + \frac{\bar{h}_1}{C_{p_{\text{ma}}}} dA\left(\omega_2 - \omega_1\right) \tag{8}$$

$$dQ_H = \frac{\bar{h}_1}{C_{p_{\text{ma}}}} dA\left\{C_{p_{\text{ma}}}\left(T_2 - T_1\right) + \left(\omega_2 - \omega_1\right) h_{\text{fg}_{@T_2}}\right\} \tag{9}$$

$$dQ_H = \frac{\bar{h}_1}{C_{p_{ma}}} dA\left\{\left(C_{p_{\text{ma}}} T_2 + \omega_2 h_{\text{fg}_{@T_2}}\right) - \left(C_{p_{\text{ma}}} T_1 + \omega_1 h_{\text{fg}_{@T_2}}\right)\right\} \tag{10}$$

Expressing enthalpy of moist air as:

$$h = h_a + h_{\text{wv}} = C_{\text{pa}} T + \omega\left(h_{\text{fg}} + C_{\text{p}_{\text{wv}}} T\right) \tag{11}$$

where specific heat of moist air is:

$$C_{p_{\text{ma}}} = \left(C_{\text{pa}} + \omega C_{p_{\text{wv}}}\right) \tag{12}$$

$$h = C_{p_{\text{ma}}} T + \omega h_{\text{fg}} \tag{13}$$

At saturation point, wet-bulb temperature is the same as dry-bulb temperature. So, rewriting enthalpy of moist air as a function of its wet-bulb temperature we get:

$$h = C_{p_{\text{ma}}} T^{\text{wb}} + \omega h_{\text{fg}_{@T^{\text{wb}}}} \tag{14}$$

Using Eqs. (14) in 10, we get:

$$dQ_H = \frac{\bar{h}_1}{C_{p_{\text{ma}}}} dA\left(h_2 - h_1\right) \tag{15}$$

As discussed in Liu et al. [27], assuming a linear relationship between the enthalpy of saturated air and wet bulb temperature over a small temperature range:

$$h = h_{\text{ref}} + Z\left(T^{\text{wb}} - T_{\text{ref}}^{\text{wb}}\right) \tag{16}$$

On substituting Eqs. (16) into (15), we finally get:

$$dQ_H = \frac{\bar{h}_1}{C_{p_{\text{ma}}}} ZdA\left(T_2^{\text{wb}} - T_1^{\text{wb}}\right) \tag{17}$$

Correlation for enthalpy of saturated air as a function of its wet-bulb temperature has built using data from ASHRAE [30]:

$$h = 0.000009\text{Ti}_{\text{bc}}^5 - 0.0016\text{Ti}_{\text{bc}}^4 + 0.1058\text{Ti}_{\text{bc}}^3 - 2.8779_{\text{bc}}^2 + 31.38\text{Ti}_{\text{bc}} - 55.27 \tag{18}$$

2.2. Bubble column condenser

In the bubble column condenser, the water level in the column is maintained up to a certain height. Moist air from humidifier after heat addition enters the bubble column through sparger. As moist air is purged uniformly in the water column, in accordance with experimental evidence [25], the water in the column is assumed as isothermal fluid. As discussed in Tow and Lienhard [25], gas side resistance is neglected as the temperature difference across the thin boundary layer outside the bubble is small compared to the temperature difference inside the bubble. Also, thermal conductivity and diffusivity of water are much higher than air. Due to the small hydrostatic pressure drop in a short column, all properties are calculated at atmospheric pressure [25]. The column is assumed to operate under steady-state conditions, and heat losses to the ambient are considered negligible and ignored. Total heat liberated during condensation is the sum of sensible heat transfer by dry air and water vapor plus latent heat of condensation released by water vapor.

$$Q_{\text{BC}} = \dot{m}_{\text{da}}\left[h_{\text{da}}\left(T_{i,\text{BC}}\right) - h_{\text{da}}\left(T_C\right)\right] + \dot{m}_{w,i}\left[h_w\left(T_{i,\text{BC}}\right) - h_{\text{wv}}\left(T_C\right)\right] + \dot{m}_{\text{cond}}\left[h_{\text{fg}}\left(T_C\right)\right] \tag{19}$$

Applying mass balance to bubble column:

$$\dot{m}_{w,i} = \dot{m}_{w,o} + \dot{m}_{\text{cond}} \tag{20}$$

Mass flow rate of moist air is given as:

$$\dot{m}_{\text{ma},i} = \rho_{\text{ma},i}\dot{V}_{\text{ma},i} = \dot{m}_{\text{da}} + \dot{m}_{w,i} \tag{21}$$

Assuming moist air is fully saturated before and after dehumidifier, Eq. (22) gives outlet mole fraction of saturated air.

$$x_0 = \frac{P_{\text{sat}}\left(T_c\right)}{P_{\text{atm}}} = \frac{\frac{\dot{m}_{w,o}}{M_w}}{\frac{\dot{m}_{w,o}}{M_w} + \frac{\dot{m}_{\text{da}}}{M_{\text{da}}}} \tag{22}$$

Heat transfer coefficient in bubble column [24] is given by the expression:

$$\bar{h}_{\text{BC}} = 0.1k_f^{1/2}\rho_f^{3/4}C_{P_f}^{1/2}\mu_f^{-1/4}g^{1/4}u_g^{1/4} \tag{23}$$

It should be noted that the bubble-column heat transfer coefficient used here is based on full-length bubble-column (with cooling wall along the enclosure sure) as proposed by Deckwer [26]. This correlation was used by Tow and Lienhard [24] successfully for predicting bubble-column dehumidifier with a cooling coil immersed inside. In such a set-up, the bubble generated may impact the cooling coil, and vigorous splashing is expected. The bubble-column model predictions were compared against the experimental data published by Tow and Lienhard [24]. Figs. 3a and b show the predicted heat flux (solid lines) as a function air temperature (entering the bubble-column) and moist airflow rates, respectively. Experimental data from Tow and Lienhard [24] is also plotted as open-circles in Fig. 3. It can be seen that the model predictions are good and are within the experimental uncertainty reported by Tow and Lienhard [24].

2.3. HDH system

Applying energy balance to a control volume of the complete HDH system (Figs. 2, 4 and 5), we get:

$$\dot{E}_{\text{in}} - \dot{E}_{\text{out}} + \dot{E}_{\text{gen}} = 0 \tag{24}$$

$$\dot{m}_c C_{p,c} T_c + \dot{m}_h C_{p,h} T_h - \begin{bmatrix} \dot{m}_c C_{p,c} T_c + \frac{d}{dy}\left(\dot{m}_c C_{p,c} T_c\right)dy + \\ \dot{m}_h C_{p,h} T_h + \frac{d}{dy}\left(\dot{m}_h C_{p,h} T_h\right)dy \end{bmatrix} \text{s} + Q_{\text{gen}} = 0 \tag{25}$$

$$-\dot{m}_c C_{p,c} dT_c - \dot{m}_h C_{p,h} dT_h + Q_{\text{gen}} = 0 \tag{26}$$

$$Q_{\text{gen}} = \dot{m}_c C_{p,c} dT_c + \dot{m}_h C_{p,h} dT_h \tag{27}$$

Energy balance for the cold stream can be written as:

$$dQ + \dot{m}_c C_{p,c} T_c - \left[\dot{m}_c C_{p,c} T_c + \frac{d}{dy}\left(\dot{m}_c C_{p,c} T_c\right)dy\right] = 0 \tag{28}$$

$$dQ = \dot{m}_c C_{p,c} dT_c \tag{29}$$

Similarly, energy balance for the hot stream is:

$$\dot{m}_h C_{p,h} T_h - \left[\dot{m}_h C_{p,h} T_h + \frac{d}{dy}\left(\dot{m}_h C_{p,h} T_h\right)dy\right] - dQ + Q_{\text{gen}} = 0 \tag{30}$$

$$dQ = -\dot{m}_h C_{p,h} dT_h + Q_{\text{gen}} \tag{31}$$

For heat transfer, the driving parameter is the temperature difference available at that location between the hot and cold streams:

$$dQ = ULdy\left(T_h - T_c\right) \tag{32}$$

Equating Eqs. (29) with (32), we get:

$$\dot{m}_c C_{p,c} dT_c = ULdy\left(T_h - T_c\right) \tag{33}$$

$$dT_c = \frac{ULdy\left(T_h - T_c\right)}{\dot{m}_c C_{p,c}} \tag{34}$$

Similarly, for the hot stream:

$$ULdy\left(T_h - T_c\right) = -\dot{m}_h C_{p,h} dT_h + Q_{\text{gen}} \tag{35}$$

$$dT_h = \frac{Q_{\text{gen}} - ULdy\left(T_h - T_c\right)}{\dot{m}_h C_{p,h}} \tag{36}$$

Subtracting Eqs. (34) from (36), we get:

$$dT_h - dT_c = \frac{Q_{\text{gen}} - ULdy\left(T_h - T_c\right)}{\dot{m}_h C_{p,h}} - \frac{ULdy\left(T_h - T_c\right)}{\dot{m}_c C_{p,c}} \tag{37}$$

Dividing the above equation by "*dy*," we obtain:

$$\frac{dT_h - dT_c}{dy} = \frac{Q_{\text{gen}}}{\dot{m}_h C_{p,h} dy} - \frac{UL\left(T_h - T_c\right)}{\dot{m}_h C_{p,h}} - \frac{UL\left(T_h - T_c\right)}{\dot{m}_c C_{p,c}} \tag{38}$$

$$\frac{d\left(T_h - T_c\right)}{dy} = \frac{Q_{\text{gen}}}{\dot{m}_h C_{p,h} dy} - UL\left[\frac{1}{\dot{m}_h C_{p,h}} + \frac{1}{\dot{m}_c C_{p,c}}\right]\left(T_h - T_c\right) \tag{39}$$

Assuming uniform heat generation, we can write $q_{\text{gen}} = Q_{\text{gen}}(dy/H)$ and using that in the above equation:

$$c_1 = \frac{q_{\text{gen}}}{\dot{m}_h C_{p,h} H} \; c_2 = UL\left[\frac{1}{\dot{m}_h C_{p,h}} + \frac{1}{\dot{m}_c C_{p,c}}\right] \tag{40}$$

In the above equation, $q_{\text{gen}} = \dot{m}_{\text{produced}} h_{\text{fg}}$:

$$\frac{d\left(T_h - T_c\right)}{dy} + c_2\left(T_h - T_c\right) = c_1 \tag{41}$$

Eq. (41) is a first-order linear differential equation and a solution can be obtained using the integrating factor method. This solution is given by the following expression:

$$\left(T_h - T_c\right)e^{c_2 y} = \frac{c_1}{c_2} e^{c_2 y} + \text{constant} \tag{42}$$

Applying the boundary conditions, at $y = 0$, $T_h = T_{i,\text{bc}}$, and $T_c = T_{i,H}$, we finally obtain the temperature difference variation along the partitioning wall as:

$$\left(T_h - T_c\right) = \frac{c_1}{c_2} + \left[\left(T_{i,bc} - T_{i,H}\right) - \frac{c_1}{c_2}\right] e^{-c_2 y} \tag{43}$$

Above equation allows prediction of variation of temperature difference across the humidifier–dehumidifier common wall as a function of vertical wall distance. For the analysis of co-flow heat exchanger heat capacity rates are treated similar to the discussion in Liu et al. [27] and are given as:

$$C_c = \dot{m}_{\text{air}} Z \tag{44}$$

$$C_h = \dot{m}_{\text{sat,air}} C_{p,\text{ma}} \tag{45}$$

The equation for the overall heat transfer coefficient is given as:

$$\frac{1}{U} = \frac{C_{p_{\text{ma}}}}{h_1 Z} + \frac{\delta_{\text{water}}}{k_{\text{water}}} + \frac{t_{\text{wall}}}{k_{\text{wall}}} + \frac{1}{h_{\text{BC}}} \tag{46}$$

As discussed in Liu et al. [27], the term $h_1 Z/C_{p_{\text{ma}}}$ is similar to a prescribed local heat transfer coefficient for convective heat transfer. Instead of using a fixed value of Z, an iterative procedure is adopted here following Liu et al. [27]. For the dry heat transfer coefficient, h_1, Gnielinski correlation [31] was used. The friction factor needed for estimating h_1 was obtained using the Petukhov's friction factor correlation [31]. The procedure used to find Z iteratively is shown in Fig. 6 and can be summarized as follows:

- Using known inlet conditions, a guess value of Z initiates the iterative loop.
- Applying modified effectiveness-NTU (number of transfer units) method, humidifier outlet temperature, bubble column inlet, and exit temperatures, specific enthalpy of moist air at humidifier inlet and exit are determined.
- The new value of Z using Eq. (16) is calculated.
- This calculated value is compared against the guess value and proceed forward if converged else procedure is iterated with calculated Z as the new guess value.

Finally, for a typical HDH cycle, GOR, which is the measure of energy efficiency of the system is defined as the ratio of latent heat of water produced to the amount of heat input. This can be expressed as:

$$\text{GOR} = \frac{\dot{m}_d h_{\text{fg}}\left(T_{\text{atm}}\right)}{\text{Q}} \tag{47}$$

3. Experimental set-up

Fig. 7a shows the schematic description of a single cell of the proposed HDH concept. Fig. 7b shows the CAD model of the prototype with two dehumidifiers sandwiching a humidifier in the center. Airflow enters through the center and is distributed via branching tubes. Feedwater enters from the top and falls along the walls while air flows in a counter-flow direction. A stainless steel screen (40 mesh) was laid on both the walls to maintain a constant water film thickness. Air from blower supplied to humidifier through 1.5 inch PVC pipe. Subsequently, air enters through four smaller PVC pipes of a nominal diameter of 20 mm.

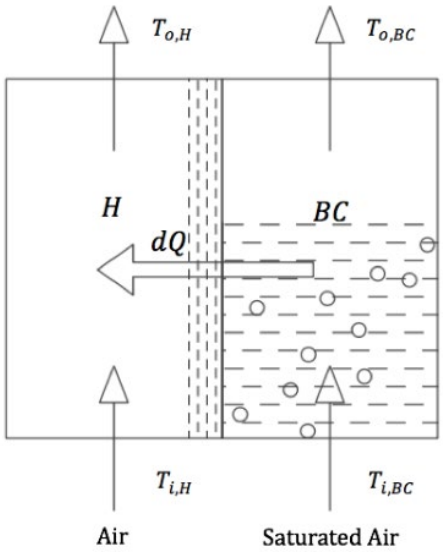

Fig. 2. Schematic of HDH system.

Air after entering humidifier (59 cm × 3 cm) from bottom passes through a bed of marbles kept at the bottom for uniform distribution of air. Saline water is supplied from the top through two *U*-shaped aluminum channel. Water not evaporated is collected from the bottom. For all the experimental data reported here, tap water was used. Air leaving humidifier contains a higher percentage of moisture. The moist air then passes through the heat exchanger (Fig. 7d), where heat is added. Air leaving the heat exchanger is at high temperature and bubbled through a bubble column condenser through a sparger plate. Bubble column condenser (Fig. 7c) contains a sparger plate and water column above it. The air pressure is kept higher than the water column pressure to allow bubbling of air through the liquid. The design of the sparger plate decides the size and velocity of the rising bubble. Improper selection of sparger leads to weeping phenomena, which results in undesirable residence time, higher pressure drop, and non-uniformity in sparging. Since weeping is an undesirable phenomenon, sparger should be operated above the critical weep velocity. Correlation for critical weep velocity from Kulkarni and Joshi [32] was used for sizing the sparger plate and is given by:

$$V_C^2 = \left(\frac{(\rho_L - \rho_G) d_o g}{\rho_G}\right)\left(0.37 + 140 H_L \left(\frac{\Delta x}{d_o}\right)^{-1.6} \left(\frac{t}{d_o}\right)^{0.75}\right) \quad (48)$$

where V_c is the critical weep velocity above which the system needs to operate. For all the experiments reported here, moist airflow velocities were maintained above this value. For temperature measurements, *K*-type thermocouples were used. These thermocouples were calibrated in a Julabo oil bath whose temperature stability was ±0.5°C. It was found that the maximum percentage error was about 1.8%. Humidity was measured using a DHT22/AM2302 digital humidity sensor whose working rage was 0%–100% RH, and precision was ±2% RH. An Arduino Uno microcontroller board was programmed to read sensor output. Airflow velocity was measured using the Generic GM8901 anemometer. The velocity range for this equipment was 0–45 m/s, with a resolution of 0.1 m/s and an accuracy of ±3%.

4. Results and discussion

Fig. 8 shows the predicted variation in driving temperature difference across the common heat transfer wall between humidifier and dehumidifier as a function of vertical distance (along *y*-direction) from the bottom ($y = 0$) using Eq. (43). For the predicted temperature variation, the volume flow rate of air was held constant at 11.5 L/s, and the water flow rate was maintained at 70 mL/min, that is, the air-to-water mass flow rate ratio of 11.4 and humidifier inlet was specified as 35°C at 65% RH. At $y = 0$, the maximum temperature difference between air entering humidifier and hot moist air entering bubble-column dehumidifier is plotted. Heat input to the system was varied to achieve

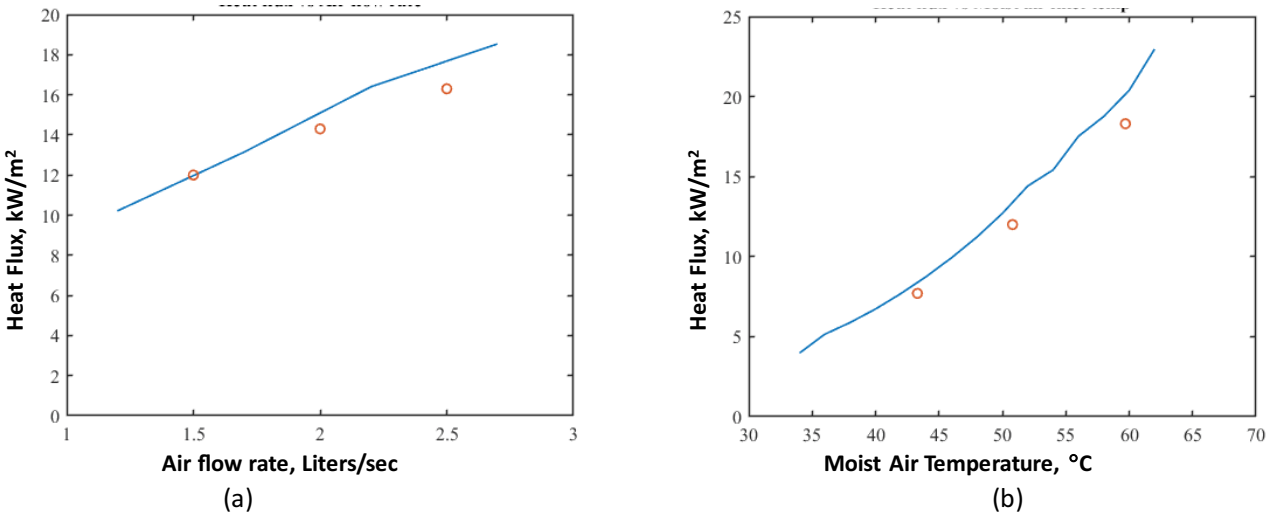

Fig. 3. Comparison between predicted and experimentally measured heat flux vs. (a) air flow rate, and (b) moist airflow temperature. Model predictions are shown as solid lines, while the experimental data is depicted by open circles.

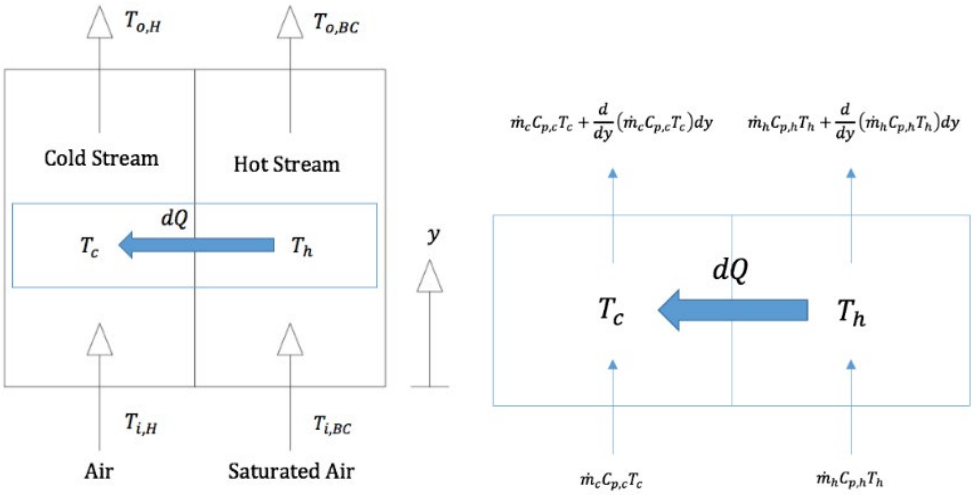

Fig. 4. Schematic of the heat exchanger with small elemental control volume.

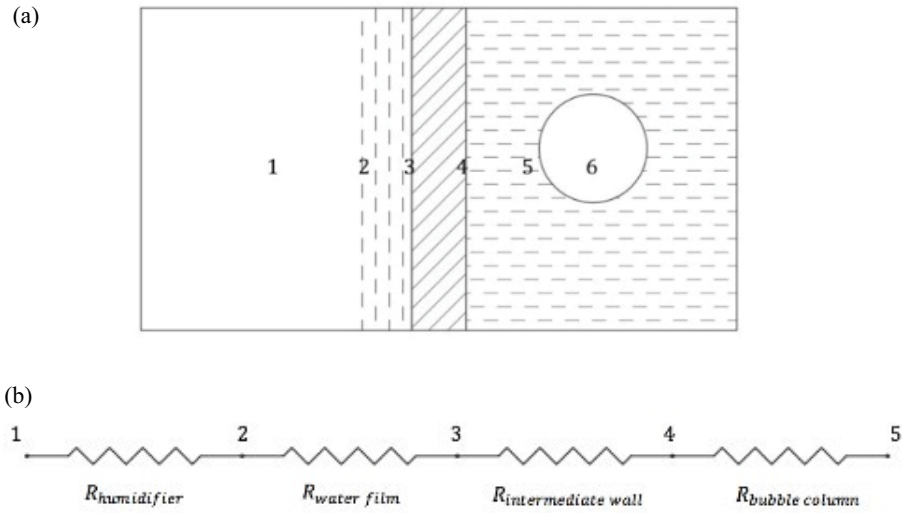

Fig. 5. (a) Schematic of control volume of HDH system where 1 refers to incoming air stream in the humidifier, 2–3 is feed water falling film, 3–4 is common wall shared by humidifier and dehumidifier, 4–5 is dehumidifier bulk liquid (produced water), and 5–6 is bubbled hot moist air and (b)corresponding thermal resistance network.

the initial temperature driving force across the humidifier–dehumidifier. It can be observed that because of the exponential nature of Eq. (43), the initial temperature difference decreases dramatically in a relatively short distance, and this effect is more pronounced at higher heat input into the system. For 320 W input into the system, about ~15°C drops within 10 cm. This suggests that evaporation rates are expected to be much lower for taller humidifiers. Also, this illustrates the impact of the co-flow arrangement discussed in this system. Owing to the nature of airflow direction in humidifier and bubble-column dehumidifier, achieving counter-flow is challenging. Hence, multi-staging of shallow bubble column may provide better performance and maintain approximately constant temperature driving forces across the common heat transfer wall.

Fig. 9 shows the predicted GOR as a function of temperature difference at $y = 0$, that is, the initial temperature difference between humidifier inlet and dehumidifier outlet, for three different MRs. GOR is a non-dimensional parameter that measures energy efficiency. Mass flow rate ratio (MR) is the non-dimensional parameter that defines flow input to the HDH system. It is the ratio of the mass flow rate of air entering the system to the mass flow rate of saline water entering the system. GOR value increases with an increase in mass flow rate ratio and initial temperature difference. Larger temperature difference drives higher heat transfer across the wall and hence a higher evaporation rate in the humidifier. Because of the larger temperature difference, energy recovered is also high, which indeed improves GOR because reduced heat input to evaporate water in the humidifier.

In order to understand the impact of latent heat of condensation released in the dehumidifier, Fig. 10 plots the overall heat transfer coefficient (U) predicted by Eq. (46) as

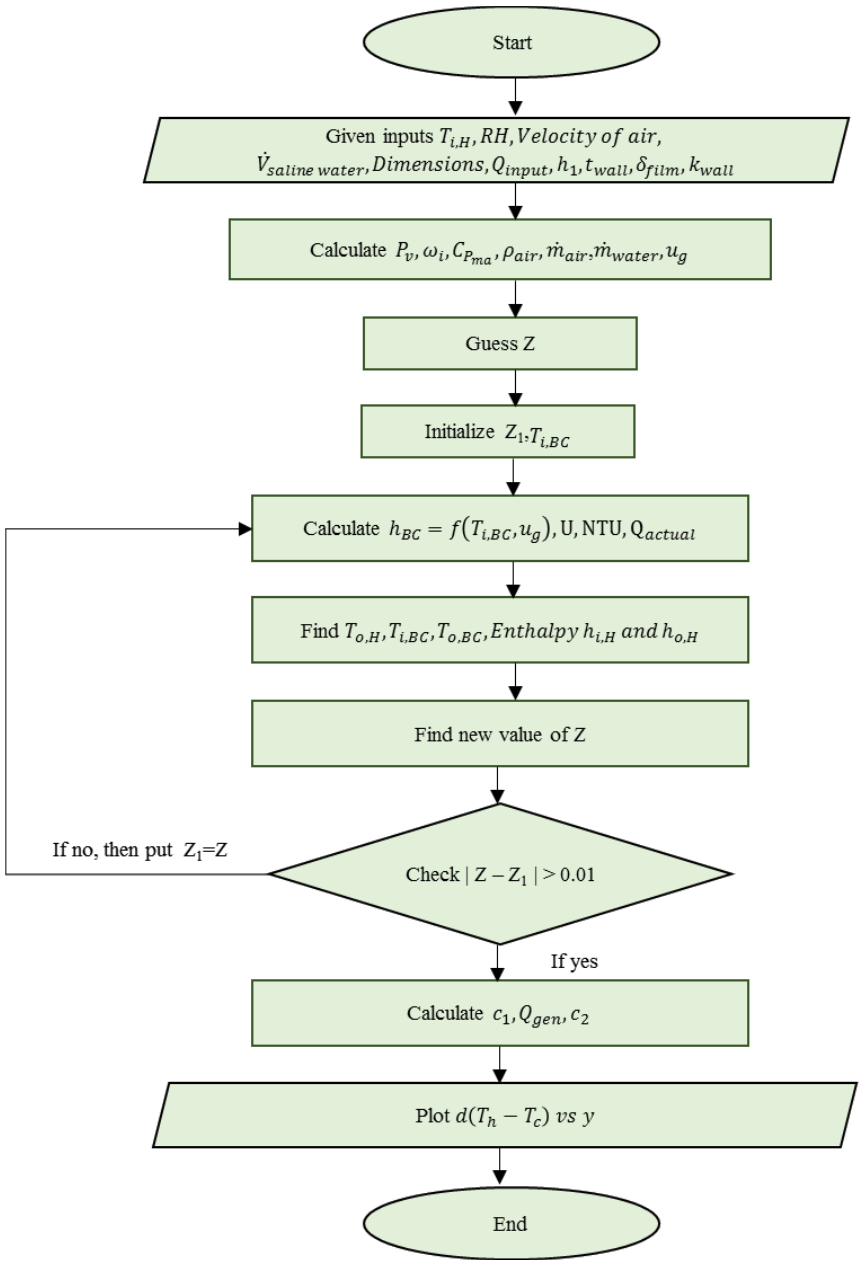

Fig. 6. Algorithm for variation of temperature difference with vertical distance.

a function of the ratio of heat release rate and heat removal rate at the wall. If $q_{gen}/Q < 1$, then the heat transfer rate exceeds the source heat transfer rate, and high heat transfer coefficients are achieved, that is, a steep increase in U. However, for $q_{gen}/Q > 1$, the drop in overall heat transfer values are more gradual and starts to asymptote towards a constant value. This indicates that heat transfer limitations begin to dominate overall performance for $q_{gen}/Q > 1$.

Fig. 11 compares the experimentally measured GOR against predicted GOR values for different test runs (Table 1). Experiments were limited to MR > 5 owing to set-up limitations. For all the experiments, the mass flow rate of air was kept constant at ~0.013 kg/s, and water flow and heat input to the system was varied. Using the method discussed by Moffat [33], an uncertainty analysis was carried out, and error bars are included for the experimental data in Fig. 11. The input parameters of the experiments are listed in Table 1. An effective water film thickness of 1.2 mm was used for humidifier modeling based on the falling film water flow rate and due to the presence of wire mesh.

Based on the flow regime map discussed in Tow and Lienhard [25] for bubble-column condensers, up to 4 cm height of the bubble-column, the authors witnessed a splashing regime. For a height of 4–6 cm, the flow was in the sloshing regime. Except case #2, all the experiments carried out had a column height of less than 4 cm, which indicates that the flow regime expected is a splashing regime. It was observed during experiments that there was

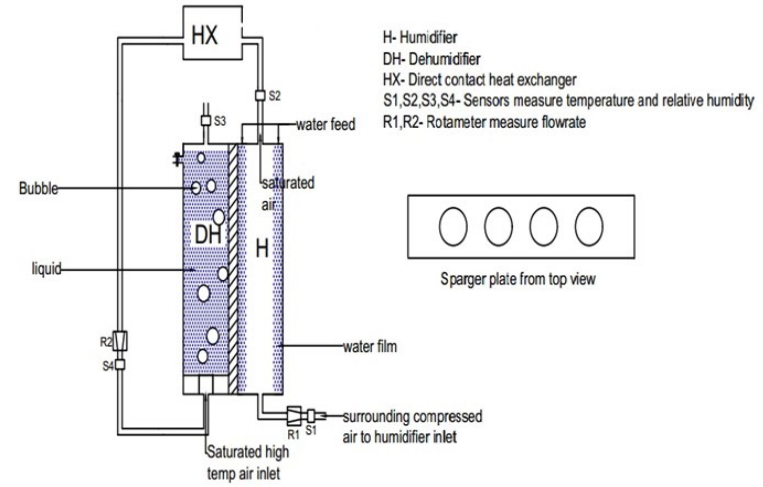

(a)

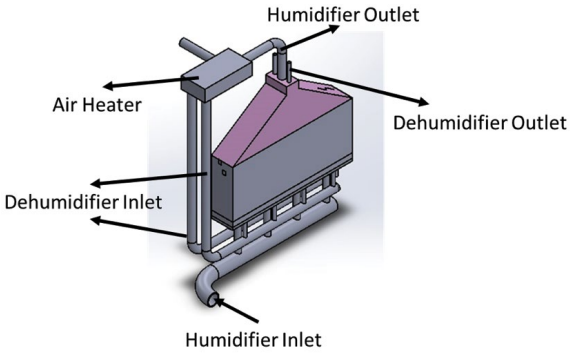

(b)

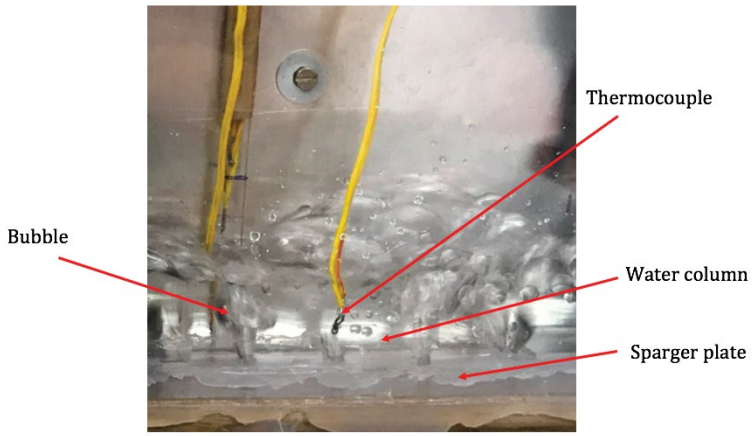

(c)

(d)

Fig. 7. (a) Schematic illustration of the experimental set-up for a single-cell, (b) three-dimensional CAD model of the experimental set-up, (c) bubble-column condenser, and (d) helical-fin heat exchanger (hot water flows through the inner pipe, and moist air flows outside).

Table 1
Experimental parameters used in this study

Description	Saline feed flow rate, mL/min	Humidifier inlet temperature, °C	Humidifier inlet RH, %	Heat input, W
Case #1	144	36.5	63.9	220
Case #2	144	38.5	63.9	279
Case #3	64	37.4	63.9	293
Case #4	70	37	64.9	316
Case #5	106.7	39.3	56	386
Case #6	87.7	39.2	57.5	307

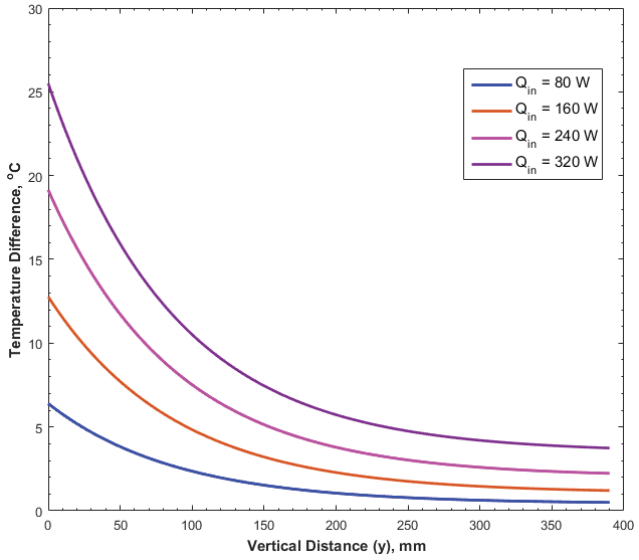

Fig. 8. Variation of temperature difference with the height of HDH system from the bottom.

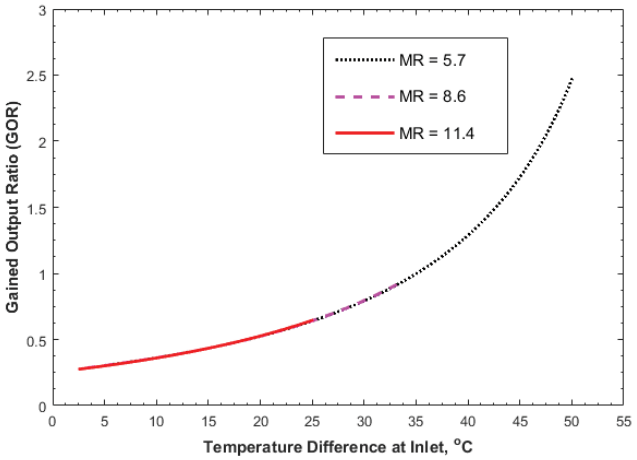

Fig. 9. Predicted GOR as a function of temperature difference at humidifier and dehumidifier inlets.

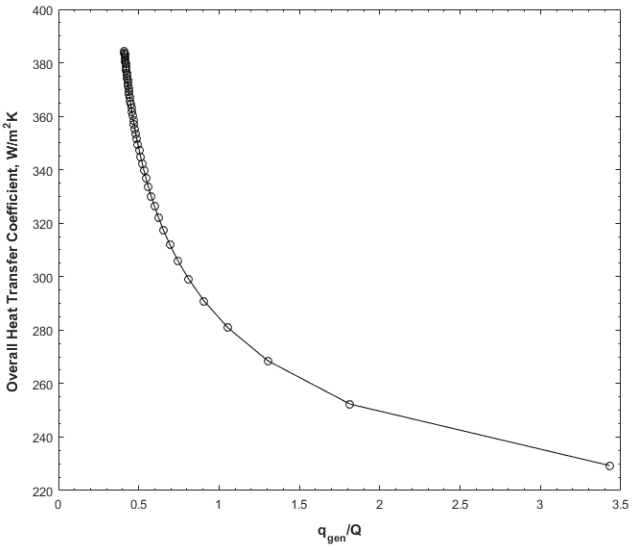

Fig. 10. Predicted overall heat transfer coefficient (U) vs. $q_{ge}n/Q$.

a carry-over of liquid drops during experiments due to the splashing flow regime. For very short bubble columns, heat transfer coefficient predicted by Eq. (22) is not expected to be accurate. Deviation of the model from the experimental data might be due to the inability to capture water film thickness (at lower water flow rates) in the humidifier section, very short bubble-column effects as well as due to environmental heat losses. Also, the empirical correlations used for calculated heat transfer coefficients play a significant role. At lower water flow rates, flow distribution in the humidifier was affected, and such flow non-uniformity was not accounted for in the present model. The inability of the model to capture a very short bubble-column effect can be seen from case #5. Indeed the experimental data is suspect as the predict GOR data carries almost 82% error. Similarly, case #2 depicts a case where bubble-column height was 4 cm. As discussed in Tow and Lienhard [25], this corresponds to the splashing–sloshing regime. Bubble coalescence and impact phenomena discussed in Tow and Lienhard [25], is expected to play a significant role. In the present work, the heat transfer wall (cooling plane) is along the side, and short bubble-columns are used. For modeling purposes, it is assumed that Deckwer's correlation is approximately valid for short bubble-column even though it was developed for full-length bubble-columns. This follows directly from the successful implementation of Deckwer's correlation by Tow and Lienhard [24] for their bubble-column condenser

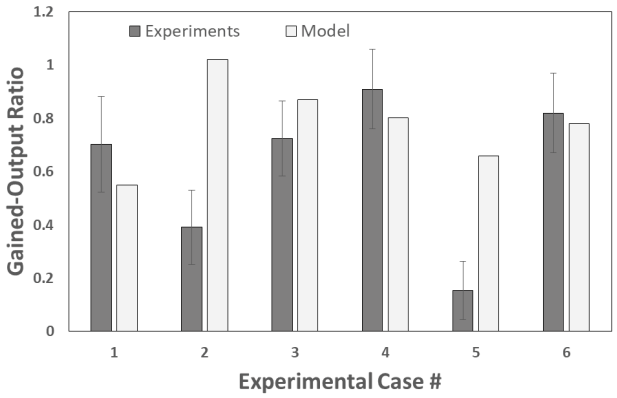

Fig. 11. Predicted and experimentally measured gained-output ratio (GOR).

modeling. For shallow bubble-column condenser, Tow and Lienhard [25] observed that the heat transfer coefficients for splashing and coalescing with bubble impact to be highest while the heat transfer coefficient for splashing and coalescing without bubble impact to be lowest. In the present case, the cooling wall is along the side, and hence chances of direct bubble impact are lower, and the heat transfer coefficient expected is to be slightly lower.

Theoretical values of GOR predicted by Hamieh and Beckman [19] were as high as 9.5 for seawater feed and up to 16.8 for brackish water. Their system concept is based on a counter-flow dewvaporation technique. In this work, due to co-flow arrangement and due to single-stage bubble-column dehumidifier is modeled, expected GORs are low. GOR may increase as we approach lower MR values, but due to experimental limitations, MR below 5.5 was not attempted.

5. Conclusions

In this paper, a combined bubble-column dehumidifier separated by a common heat transfer wall from a falling-film humidifier was studied both by theoretical analysis as well as with simple prototype experiments. A modified heat exchanger analysis was carried out that accounts for the volumetric heat generation in the dehumidifier (due to the release of latent of condensation of water vapor) that exchanges heat with a falling-film humidifier. Temperature difference evolution, the impact of MR, overall heat transfer coefficient, and energy efficiency (GOR) of the proposed approach were discussed using the developed model.

While shallow bubble-column dehumidifier provided compactness, the overall performance was limited due to the co-flow arrangement of humidifier/dehumidifier. The co-flow arrangement enables large temperature differences at the inlet, and this temperature drops quickly over a short distance. In order to mimic a counter-flow arrangement, that is, constant temperature difference across streams, a multi-staged bubble-column dehumidifier on one-side with a falling film humidifier on the other side might be appropriate. Also, to achieve a higher heat transfer coefficient source rate of heat generation should be less than the heat removal rate at the common wall. Future work will attempt to capitalize on the aforementioned insights from the current work.

Nomenclature

C_p	—	Specific heat capacity, J/kg K
g	—	Acceleration due to gravity, m/s^2
h_{fg}	—	Latent heat of vaporization, J/kg
h	—	Specific enthalpy, J/kg K
$\bar{h}_1$	—	Heat transfer coefficient of air, W/m^2 K
$\bar{h}_m$	—	Mass transfer coefficient, kg/m^{2}s
k	—	Thermal conductivity, W/m K
L	—	Length, m
M	—	Molecular weight
P	—	Pressure, Pa
Q	—	Heat transfer rate, W
t	—	Common wall thickness, m
T	—	Temperature, °C
U	—	Overall heat transfer coefficient, W/m^2 K
$\dot{V}$	—	Volume flow rate, m^3/s
Z	—	Ratio of enthalpy changes versus wet-bulb temperature, J/kg K
δ_{water}	—	Water film thickness, mm
ω	—	Humidity ratio, kg of water vapor/kg of dry air
μ	—	Dynamic viscosity, Pa-s
ρ	—	Density, kg/m^3

Subscripts

H	—	Humidifier
BC	—	Bubble Column
cond	—	Condensation
gen	—	Generation
cond	—	Condensation
h	—	Hot
sat	—	Saturation
da	—	Dry air
w	—	Water vapor
ma	—	Moist air
f	—	Fluid
c	—	Cold, Critical
wb	—	Wet-bulb

References

[1] Available at: http://unicef.in/PressReleases/30/Water-in-India-Situation-and-Prospects
[2] R.V. Wahlgren, Atmospheric water vapor processor designs for potable water production: a review, Water Res., 35 (2001) 1–22.
[3] G.P. Narayan, J.H. Lienhard V, Chapter 9: Humidification Dehumidification Desalination, J. Kucera, Ed., Desalination: Water from Water, Wiley-Scrivener, Salem, MA, 2014, pp. 425–472.
[4] G.P. Narayan, M.H. Sharqawy, E.K. Summers, J.H. Lienhard, S.M. Zubair, M.A. Antar, The potential of solar-driven humidification-dehumidification desalination for small-scale decentralized water production, Renewable Sustainable Energy Rev., 14 (2010) 1187–1201.
[5] M.T. Ghazal, U. Atikol, F. Egelioglu, An experimental study of a solar humidifier for HDD systems, Energy Convers. Manage., 82 (2014) 250–258.
[6] A.M.I. Mohamed, N.A. El-Minshawy, Theoretical investigation of solar humidification-dehumidification desalination system

using parabolic trough concentrators, Energy Convers. Manage., 52 (2011) 3112–3119.
[7] N.A.S. Elminshawy, F.R. Siddiqui, M.F. Addas, Experimental and analytical study on productivity augmentation of a novel solar humidification–dehumidification (HDH) system, Desalination, 365 (2015) 36–45.
[8] A. Giwa, N. Akther, A. Al Housani, S. Haris, S.W. Hasan, Recent advances in humidification dehumidification (HDH) desalination processes: improved designs and productivity, Renewable Sustainable Energy Rev., 57 (2016) 929–944.
[9] F.E. Ahmed, R. Hashaikeh, N. Hilal, Solar-powered desalination – Technology, energy and future outlook, Desalination, 453 (2019) 54–76.
[10] Y. Ghalavand, M.S. Hatamipour, A. Rahimi, Humidification compression desalination, Desalination, 341 (2014) 120–125.
[11] N. Niroomand, M. Zamen, M. Amidpour, Theoretical investigation of using a direct contact dehumidifier in humidification–dehumidification desalination unit based on an open-air cycle, Desal. Water Treat., 54 (2014) 305–315.
[12] J.F. Klausner, Y. Li, R. Mei, Evaporative heat and mass transfer for the diffusion driven desalination process, Heat Mass Transfer, 42 (2005) 528–536.
[13] K. Wang, T. Hu, A.H. Hassabou, M. Spinnler, W. Polifke, Analyzing and modeling the dynamic thermal behaviors of direct contact condensers packed with PCM spheres, Continuum Mech. Thermodyn., 25 (2012) 23–41.
[14] M.K. Abu Arabi, K.V. Reddy, Performance evaluation of desalination processes based on the humidification/dehumidification cycle with different carrier gases, Desalination, 156 (2003) 281–293.
[15] M. Vlachogiannis, V. Bontozoglou, C. Georgalas, G. Litinas, Desalination by mechanical compression of humid air, Desalination, 122 (1999) 35–42.
[16] S.A. Nada, H.F. Elattar, A. Fouda, Experimental study for hybrid humidification–dehumidification water desalination and air conditioning system, Desalination, 363 (2015) 112–125.
[17] R.K. McGovern, G.P. Thiel, G. Prakash Narayan, S.M. Zubair, J.H. Lienhard V, Performance limits of zero and single extraction humidification–dehumidification desalination systems, Appl. Energy, 102 (2013) 1081–1090.
[18] G.P. Narayan, M.H. Sharqawy, S. Lam, S.K. Das, J.H. Lienhard V, Bubble columns for condensation at high concentrations of noncondensable gas: heat-transfer model and experiments, AIChE J., 59 (2013) 1780–1790.
[19] B.M. Hamieh, J.R. Beckman, Seawater desalination using dewvaporation technique: theoretical development and design evolution, Desalination, 195 (2006) 1–13.
[20] B.M. Hamieh, J.R. Beckman, M.D. Ybarra, The dewvaporation tower: an experimental and theoretical study with economic analysis, Desal. Water Reuse, 10 (2000) 35–43.
[21] B.M. Hamieh, J.R. Beckman, M.D. Ybarra, Brackish and seawater desalination using a 20 ft^2 dewvaporation tower, Desalination, 140 (2001) 217–226.
[22] S. Ranganathan, Final Scientific/Technical Report for Program Title: Solar Powered Dewvaporation Desalination System, Polestar Technologies Inc., Needham Heights, MA, 2017.
[23] W.J. Minkowycz, E.M. Sparrow, Condensation heat-transfer in the presence of noncondensables: interfacial resistance, superheating, variable properties, and diffusion, Int. J. Heat Mass Transfer, 9 (1966) 1125–1144.
[24] E.W. Tow, J.H. Lienhard V, Experiments and modeling of bubble column dehumidifier performance, Int. J. Therm. Sci., 80 (2014) 65–75.
[25] E.W. Tow, J.H. Lienhard V, Heat transfer to a horizontal cylinder in a shallow bubble column, Int. J. Heat Mass Transfer, 79 (2014) 353–361.
[26] W.D. Deckwer, On the mechanism of heat transfer in bubble column reactors, Chem. Eng. Sci., 35 (1980) 1341–1346.
[27] Z. Liu, W. Allen, M. Modera, Simplified thermal modeling of indirect evaporative heat exchangers, HVAC&R Res., 19 (2013), 257–267.
[28] V. Narayanan, K. Murty, J. Jenks, Heat exchanger analysis modified to account for a heat source, J. Heat Transfer, 130 (2008) 124502.
[29] J.C. Kloppers, D.G. Kröger, The Lewis factor and its influence on the performance prediction of wet-cooling towers, Int. J. Therm. Sci., 44 (2005) 879–884.
[30] American Society of Heating, Refrigerating, and Airconditioning Engineers, 2001 ASHRAE Handbook Fundamentals, Atlanta, GA, 2001.
[31] F.P. Incropera, D.P. DeWitt, Fundamentals of Heat and Mass Transfer, 3rd ed., John Wiley & Sons, New York, NY, 1990.
[32] A.V. Kulkarni, J.B. Joshi, Design and selection of sparger for bubble column reactor. Part I: performance of different spargers, Chem. Eng. Res. Des., 89 (2011) 1972–1985.
[33] R.J. Moffat, Describing the uncertainties in experimental results, Exp. Therm. Fluid Sci., 1 (1988) 3–17.